Bipolar nanochannels: The effects of an electroosmotic instability. Part II: Time-transient response

Ramadan Abu-Rjal and Yoav Green†

Department of Mechanical Engineering, Ben-Gurion University of the Negev, Beer-Sheva 8410501, Israel

† yoavgreen@bgu.ac.il

Supplementary Materials

Contents

Supplement to main text section on unipolar systems

1.1 *Unipolar systems with symmetric diffusion layers*

In the main text and further below (Sec. 1.2), we present results for $\bar{i}(t)$ for an asymmetric unipolar system $(2L_1 = L_4)$ for $V > 0$ and $V < 0$. Before continuing to that analysis, we wish to demonstrate that for a unipolar system with symmetric diffusion layers (which were also considered in Part I), the electrical current densities, without and with EOF, are the same [except for the sign change, $\bar{i}_{V>0}(t) = -\bar{i}_{V<0}(t)$] (**Figure S1**). Naturally, $\overline{\overline{E_k}}(t)$ are identical (not shown here).

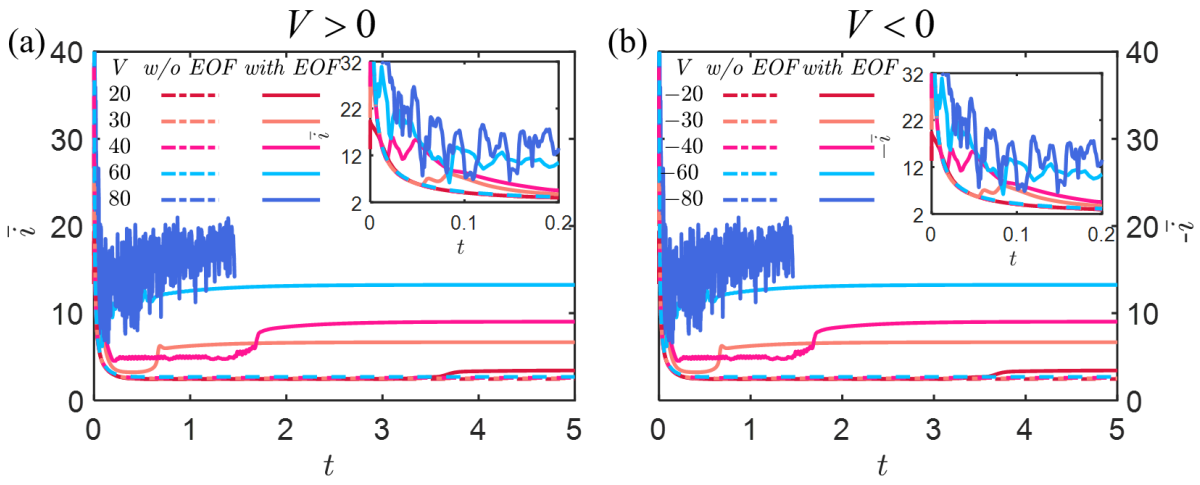

Figure S1. *Time evolution of the electrical current density, $\bar{i}(t)$, in a symmetric unipolar system ($L_1 = L_4$) for several (a) positive and (b) negative voltages, without EOF and with EOF. Note that in (b), we present $-\bar{i}(t)$. Insets: Zoom up at early times. Simulation parameters are given in* ***Table 1*** *and* ***Table 2*** *in the Supplementary Material of Part I, except that* $(L_1 = L_4)$.

1.2 *Unipolar systems with asymmetric diffusion layers*

We now turn to the case of an asymmetric unipolar system ($L_4 = 2L_1$) for several positive and negative voltages in the over-limiting current (OLC) regime. **Figure S2** plots the time evolution of the current density, $\bar{i}(t)$, and the surface average of the kinetic energy, $\overline{\overline{E_k}}(t)$. Specifically, we observe that above a threshold voltage, $V_{cr} \approx \pm 20$, both symmetric (**Figure S1**) and asymmetric systems exhibit EOI (resulting in OLC). Since we are considering an asymmetric system, the positive [**Figure S2**(a)] and negative [**Figure S2**(b)] voltage responses, regardless of whether EOF is included, are different [such that $\bar{i}(t;V) \neq -\bar{i}(t;-V)$]. This is different from the symmetric system described above (**Figure S1**). It can be observed that the current with EOF is always larger than the current without EOF and that above another critical voltage, the $\bar{i}(t)$ becomes chaotic (Demekhin, Nikitin, & Shelistov, 2013; Druzgalski, Andersen, & Mani, 2013). As can be expected, the kinetic energy, $\overline{\overline{E_k}}(t)$, increases with increasing voltage magnitude [**Figure S2**(c-d)].

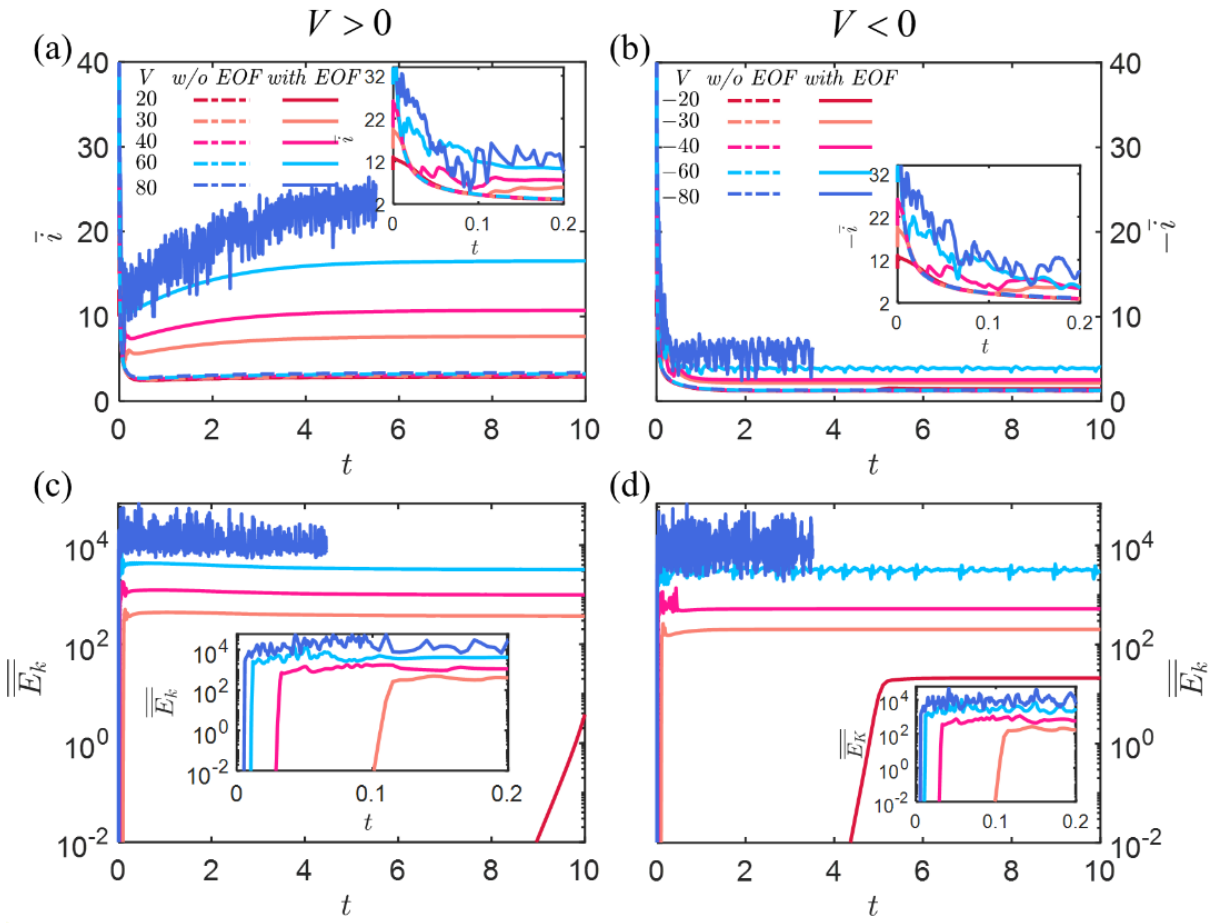

Figure S2. *(a-b) Time evolution of the electrical current density, $\bar{i}(t)$, in an asymmetric unipolar system ($2L_1 = L_4$) for several (a) positive and (b) negative voltages, without EOF and with EOF. Note that in (b), we present $-\bar{i}(t)$. (c-d) The time evolution of the surface average kinetic energy, $\overline{\overline{E_k}}(t)$, in the depleted layer for (c) positive and (d) negative voltages. Insets: Zoom up at early times.*

1.3 *EOI onset time*

Figure S3 shows that the onset time of the EOI varies between symmetric unipolar system ($L_1 = L_4$) and asymmetric unipolar system ($2L_1 = L_4$). Further, while the onset time of symmetric systems is the same for positive and negative voltages, it is not the same for asymmetric systems. It can be observed that the symmetric system has a shorter onset time – this is because the time required for the equilibrium EDL to transform to the ESC is shorter. For the sake of comparison, we have also added the ideal bipolar EOI onset time to this figure. Note that the ideal bipolar system has fewer points for $V > 0$, because EOI sets in at larger voltages, and that there are no points for $V < 0$ because EOI does not appear here.

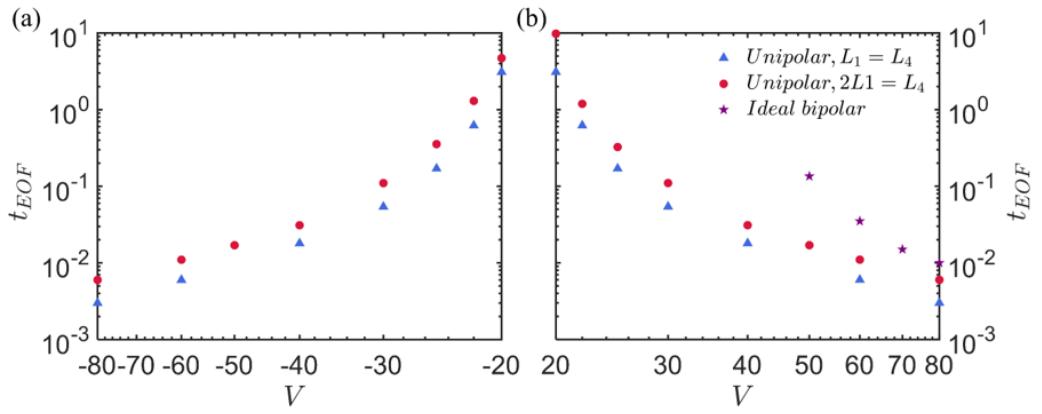

Figure S3. *Log-log plot of the EOI onset time (first local maximum in the* $\bar{i} - t$ *response) for two unipolar systems, symmetric* $(L_1 = L_4)$ *and asymmetric* $(2L_1 = L_4)$*, and an ideal bipolar system for (a) negative voltages and (b) positive voltages.*

2. Supplement to main text section on ideal bipolar systems

2.1 *Transient responses of the salt* j *and electrical* i *currents*

Figure S4 shows the time-dependent dynamics for the surface average salt current in Region 1, $\bar{\bar{j}}_1(t)$, and the electric current density, $\bar{i}(t)$. Without EOF, the changes in both fluxes are smooth, and after $\bar{i}(t)$ has reached a minimum, it increases monotonically. However, once EOF is included, the changes are no longer monotonic since both $\bar{\bar{j}}_1(t)$ and $\bar{i}(t)$ are still influenced by the instability. Only at much later times, around $t \sim 1$, when the instability completely decays, does the change in $\bar{i}(t)$ become monotonic.

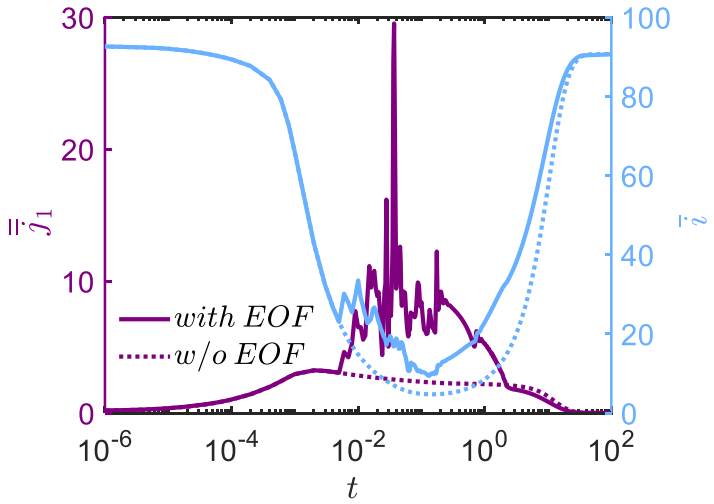

Figure S4*. Time evolution of the electric current density,* $\bar{i}(t)$*, and the surface average salt current in Region 1,* $\bar{\bar{j}}_1(t)$ *for an ideal bipolar system for the two scenarios, without and with EOF, for* $V = 100$*.*

2.2 *Response for several additional positive voltages*

Here, we demonstrate the robustness of the decay of the EOI and the eventual convergence of the $\bar{i}_{With-EOF}$ to $\bar{i}_{w/o-EOF}$ for all voltages (positive and negative). **Figure S5**(a) shows $\bar{i}(t)$ for several positive voltages with and without EOF. **Figure S5**(b) shows the difference in the current of both scenarios, $\Delta\bar{i} = \bar{i}_{With-EOF} - \bar{i}_{w/o-EOF}$, where it can be observed that the current difference always decays to zero as $\overline{\overline{E_k}}(t)$ (and the EOI) decays in Regions 1 [**Figure S5**(c)] and 4 [**Figure S5**(d)].

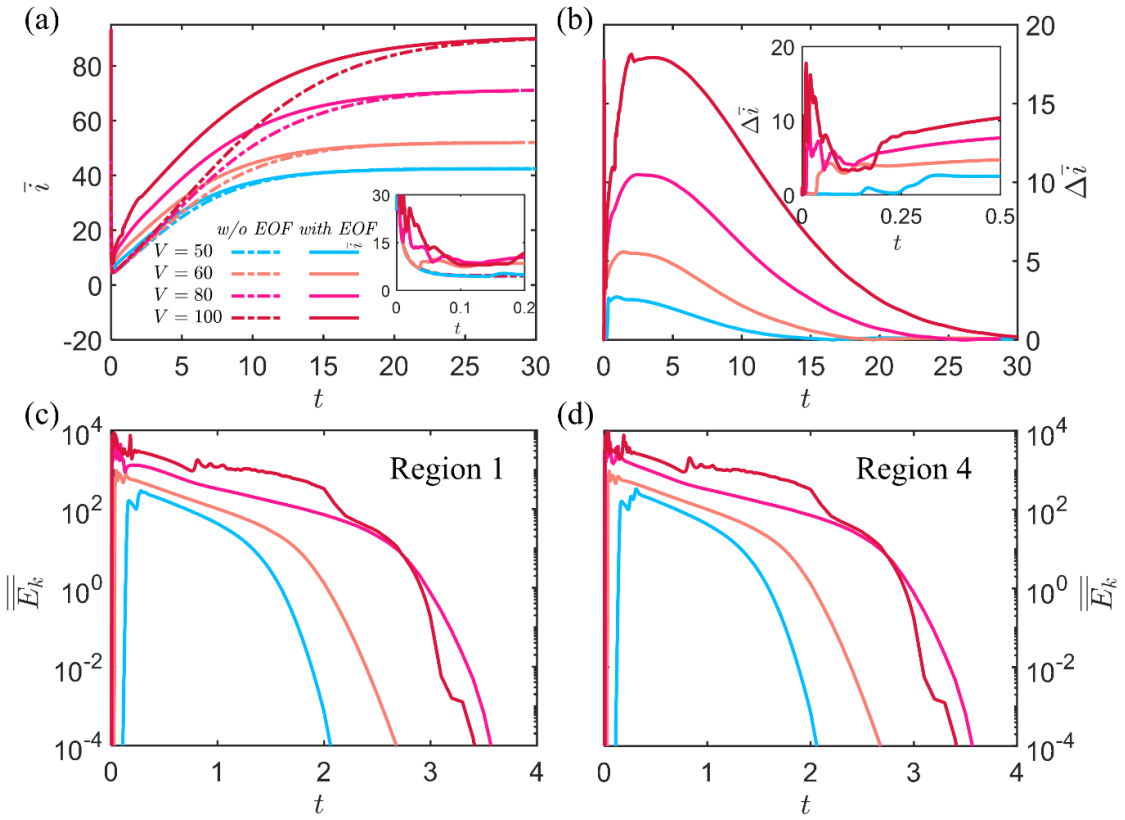

Figure S5*. (a) Time evolution of the electric current density, $\bar{i}(t)$, in an ideal bipolar system for the two scenarios, without and with EOF, for positive voltages. (b) The time-transient of the current difference $\Delta\bar{i} = \bar{i}_{With-EOF} - \bar{i}_{w/o-EOF}$ plotted in (a). Insets: Early time zoom-ups. (c-d) The surface average time-dependent kinetic energy, $\overline{\overline{E_k}}(t)$, in (c) Region 1 and (d) Region 4.*

2.3 *Response for a negative voltage*

To complete our analysis, we also considered negative voltages. For the sake of brevity, here we will only discuss the key result that for negative voltages, an ESC doesn't form, and EOI cannot appear. As a result, the current density without EOI and with EOI are identical. The reason that the ESC doesn't form was previously alluded to in our past work [see Supplement Information Sec. 2 of Abu-Rjal and Green (2021)]. Similar to how for positive voltages, we have the formation of double depletion layers [**Figure S6**(c)-(d)], then for negative voltages, we have the formation of double enriched layers [**Figure S6**(a)-(b)]. Enriched layers do not support nonequilibrium ESCs [**Figure S6**(c)-(d)]. Hence, the instability does not appear for negative voltages.

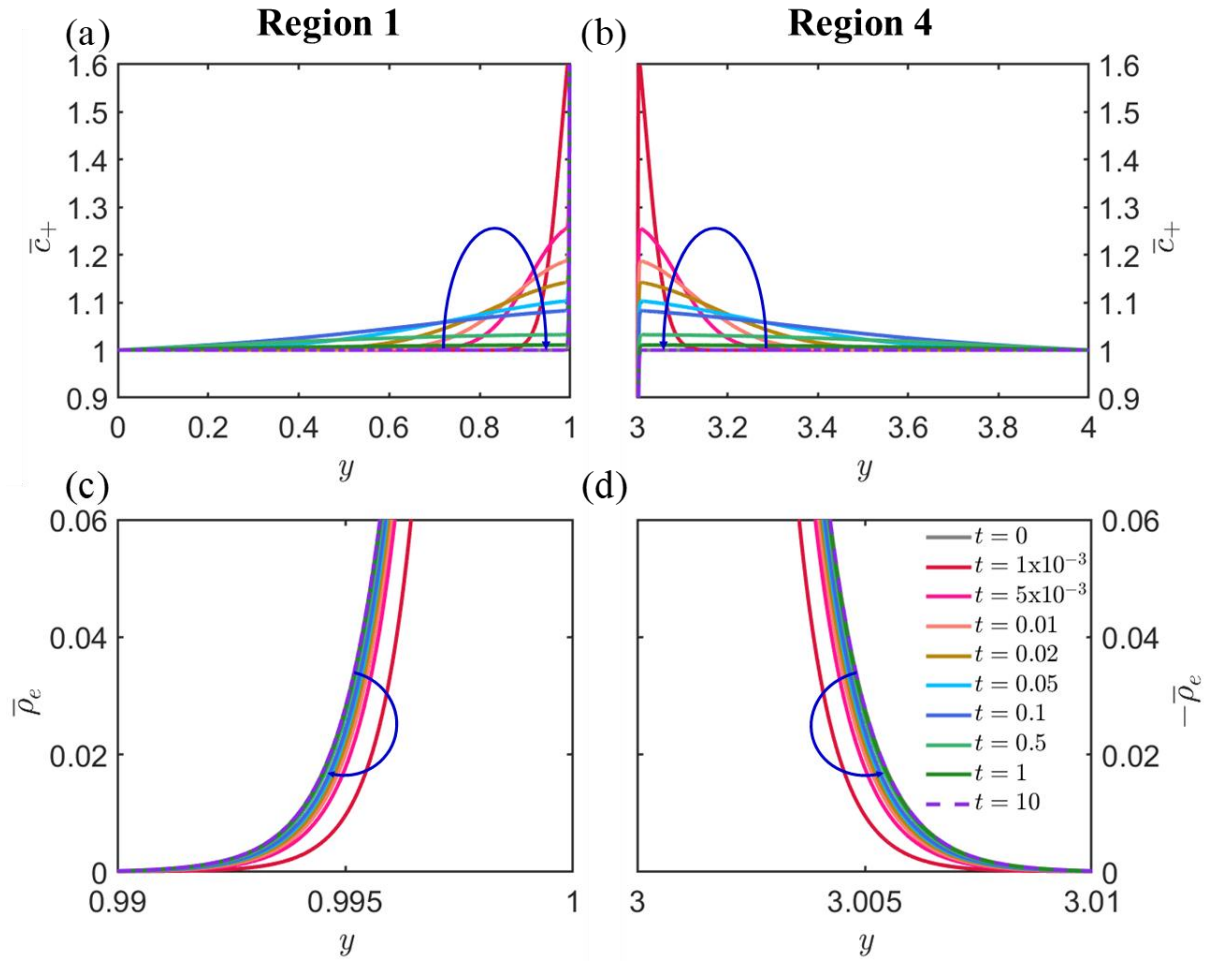

Figure S6. *The spatial-averaged time-dependent profiles of (a and b) the concentration* $\bar{c}_+$*, and (c and d) the space charge density* $\bar{\rho}_e$ *in Regions 1 and 4 of an ideal bipolar system for* $V = -100$*. Note that in (c), we present* $\bar{\rho}_e$*, while in (d), we present* $-\bar{\rho}_e$*. The legend is given in (d). The blue curved arrows indicate the direction of increasing time.*

3. Supplement to main text section on non-ideal bipolar systems

3.1 *Transient responses of the salt* j *and electrical* i *currents*

Figure S7 shows the time-dependent dynamics for the surface average salt current in Region 1, $\bar{\bar{j}}_1(t)$, Region 4, $\bar{\bar{j}}_4(t)$, and the electric current density, $\bar{i}(t)$. In contrast to what is shown for the ideal scenario (**Figure S4**), here, the steady-state salt density is not zero – resulting in different dynamics. We see that in Region 1, at steady-state $\bar{\bar{j}}_1(t)$ is still noisy – due to the instability – while in Region 4 $\bar{\bar{j}}_4(t)$ is noisy only at early times when the instability is still apparent, but at steady-state, when the instability has decayed, the flux has reached a steady-state.

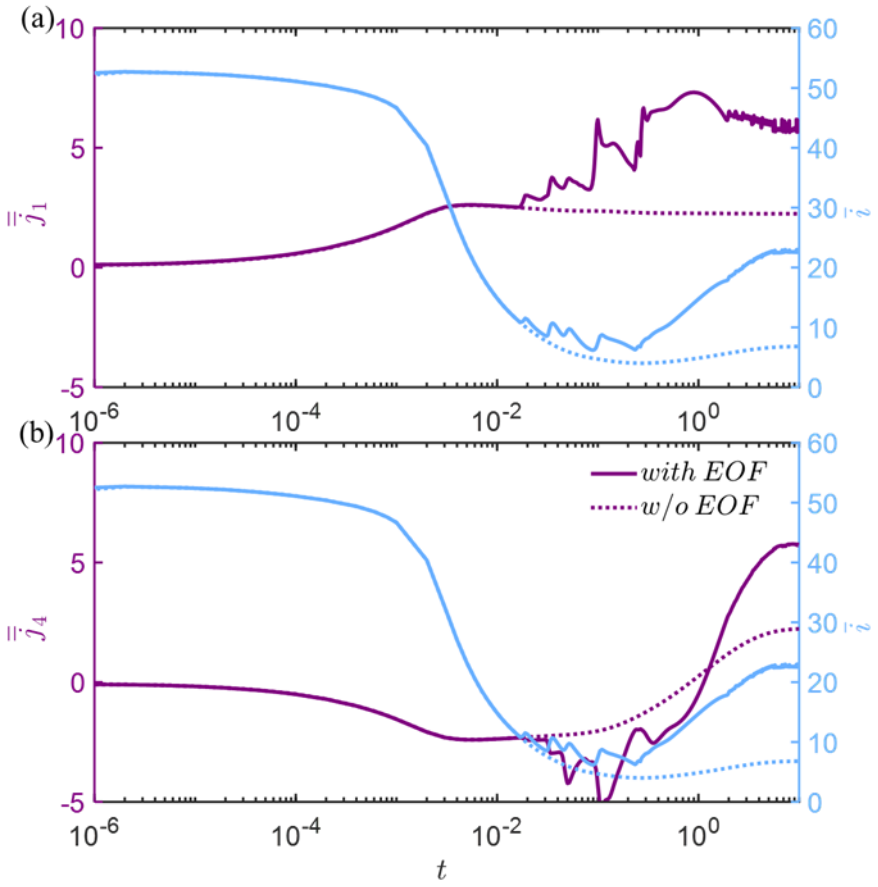

Figure S7*. Time evolution of the electric current density,* $\bar{i}(t)$*, and the surface average salt current in (a) Region 1,* $\bar{\bar{j}}_1(t)$*, and (b) Region 4,* $\bar{\bar{j}}_4(t)$*, for a non-ideal bipolar system for the two scenarios, without and with EOF, for* $V = 60$*.*

3.2 *Electrical current density and kinetic energy density for positive voltages*

Similar to the above figures, here we provide supplemental information of $\bar{i}(t)$ and $\bar{\bar{E}}_k(t)$ for several additional voltages to the configuration discussed in the main text Sec. 5. The qualitative results remain unchanged relative to those discussed in the main text ($V = 60$). Notably, **Figure S8**(a-b) shows that for all voltages, the current with EOF increases relative to the current with non-EOF. For $V \geq 60$, the steady-state current is noisy due to the appearance of a "chaotic motion" (Demekhin, Nikitin, & Shelistov, 2013; Druzgalski, Andersen, & Mani, 2013). **Figure S8**(c-d) show that as the voltage increases, the kinetic energy in Region 1 increases. The inset of **Figure S8**(c) shows that the kinetic energy, and EOI, in Region 4 decay to zero.

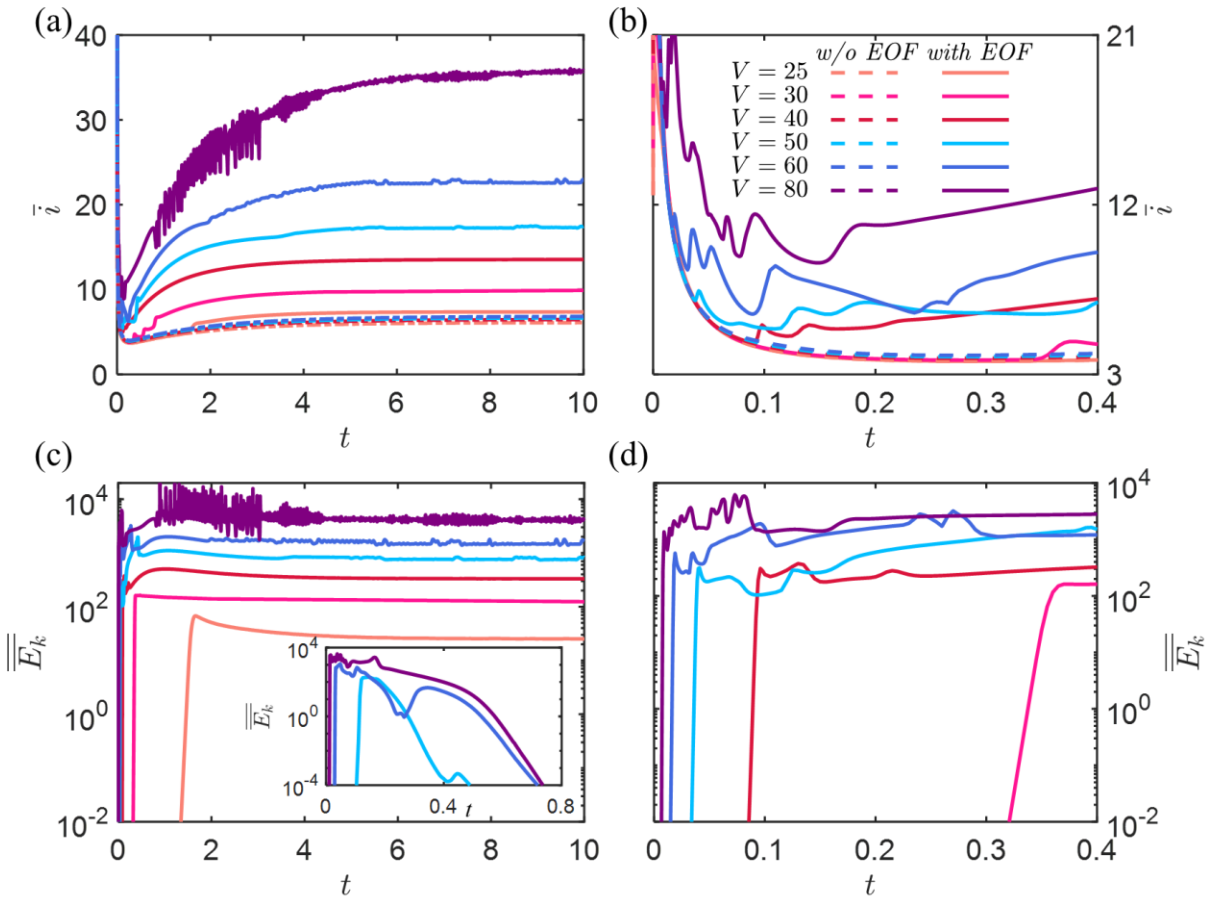

Figure S8: *(a) Time evolution of the electric current density,* $\bar{i}(t)$*, for the two scenarios: without and with EOF, upon a stepwise application of constant positive voltages for a non-ideal bipolar system. (b) Early time zoom-up of* $\bar{i}(t)$ *shown in (a). (c) Surface average time-dependent kinetic energy,* $\overline{\overline{E_k}}(t)$*, in Region 1 where the inset is* $\overline{\overline{E_k}}(t)$ *in Region 4. (d) Early time zoom-up of* $\overline{\overline{E_k}}(t)$ *in Region 1 shown in (c). Simulations parameters are* $L_{1,2,3,4}=1$*,* $N_2=25$*, and* $N_3=-10$*.*

4. Movie Description

Movie name	Section #	Description
Movie 1	Section 3	The spatial-averaged time-dependent profiles of the counterion concentration $\overline{c}_+$ and the space charge density $\overline{\rho}_e$ at Regions 1 and 4 in the unipolar simulations of **Figure 3**.
Movie 2	Section 3	Time evolution of the positive counterion concentration (2D color plot), c_+, and velocity streamlines (white lines) in Regions 1 and 4 in the unipolar simulations of **Figure 3**. The bottom plot shows the time evolution of the surface average kinetic energy, $\overline{\overline{E_k}}(t)$, in the depleted layer (Region 1).
Movie 3	Section 3	The spatial-averaged time-dependent profiles of fluxes in the unipolar system simulation of **Figure 3**.
Movie 4	Section 4	The spatial-averaged time-dependent profiles of the positive concentration $\overline{c}_+$ and the space charge density $\overline{\rho}_e$ at Regions 1 and 4 in the ideal bipolar simulations of **Figure 5**.
Movie 5	Section 4	Time evolution of the positive concentration (2D color plot), c_+, and velocity streamlines (white lines) in Regions 1 and 4 in the ideal bipolar simulations of **Figure 5**. The bottom plot shows the time evolution of the surface average kinetic energy, $\overline{\overline{E_k}}(t)$, in the diffusion layer (Regions 1 and 4).
Movie 6	Section 4	The spatial-averaged time-dependent profiles of fluxes in the ideal bipolar system simulation of **Figure 5**.
Movie 7	Section 5	The spatial-averaged time-dependent profiles of the positive concentration $\overline{c}_+$ and the space charge density $\overline{\rho}_e$ at Regions 1 and 4 in the non-ideal bipolar simulations of **Figure 7**.
Movie 8	Section 5	Time evolution of the positive concentration (2D color plot), c_+, and velocity streamlines (white lines) in Regions 1 and 4 in the non-ideal bipolar simulations of **Figure 7**. The bottom plot shows the time evolution of the surface average kinetic energy, $\overline{\overline{E_k}}(t)$, in the diffusion layer (Regions 1 and 4).
Movie 9	Section 5	The spatial-averaged time-dependent profiles of fluxes in the non-ideal bipolar system simulation of **Figure 7**.

References

Abu-Rjal, R., & Green, Y. (2021). Bipolar Nanochannels: A Systematic Approach to Asymmetric Problems. *ACS Applied Materials & Interfaces*, *13*(23), 27622–27634. https://doi.org/10.1021/acsami.1c05643

Demekhin, E. A., Nikitin, N. V., & Shelistov, V. S. (2013). Direct numerical simulation of electrokinetic instability and transition to chaotic motion. *Physics of Fluids*, *25*(12), 122001. https://doi.org/10.1063/1.4843095

Druzgalski, C. L., Andersen, M. B., & Mani, A. (2013). Direct numerical simulation of electroconvective instability and hydrodynamic chaos near an ion-selective surface. *Physics of Fluids*, *25*(11), 110804. https://doi.org/10.1063/1.4818995